Progress In Electromagnetics Research C, Vol. 51, 45–53, 2014

Design and Experiment of a Permanent Magnet Tubular Linear Generator for Wave Energy Conversion System

Zhongxian Chen and Haitao Yu*

Abstract—In this paper, flux of permanent magnet tubular linear generator (PMTLG) is modeled and analyzed. With the model, air-gap leakage flux coefficient can be expressed analytically in terms of permanent magnet dimensions and air-gap width. The validity of analytical expression of air-gap leakage flux coefficient is verified by finite element analysis (FEA) with a maximum error of 6.8%. Furthermore, longitudinal end flux's influence on the detent force of PMTLG is analyzed in detail with the model. A detent force minimization technique is deduced from the analysis results, and confirmed by FEA. Finally, after optimization of air-gap leakage flux coefficient and detent force, a PMTLG is built and experimented.

1. INTRODUCTION

Simple structure and high efficiency make PMTLG an attractive candidate of converting wave energy into electrical energy among various permanent magnet generators [1, 2]. However, the basic structure and flux of PMTLG do not share much similarity with those of rotating generators [3, 4]. Thus, flux analysis of PMTLG becomes increasingly important.

In PMTLG, air-gap leakage flux mainly consisting of two parts: magnet-to-magnet flux and magnet-to-piston flux. Air-gap leakage flux has a great influence on the utilization ratio of permanent magnet (PM) material. The former, i.e., magnet-to-magnet flux of rotating machines and interior PM machines has been well investigated [5–7]. In fact, the latter, i.e., magnet-to-piston flux also plays an important role in the calculation of air-gap leakage flux coefficient. One major work of this paper is to obtain the analytical expression of air-gap leakage flux coefficient including the above two parts of air-gap leakage flux in surface-mounted PMTLG.

Besides, longitudinal end flux has a significant influence on the detent force of PMTLG, and consequently on the dynamic performance of wave energy conversion system [8]. Detent force minimization techniques have been thoroughly studied in permanent magnet linear machine by numerical computation [9–14]. However, few papers illustrate why detent force can be minimized by these techniques. Another major work of this paper is to investigate the detent force of PMTLG including longitudinal end flux effects through an unsaturated reluctance model, and a detailed analytical expression of detent force is obtained. From the detailed analytical expression of detent force is a detent force minimization technique deduced.

The analysis results show that the analytical expression of air-gap leakage flux coefficient is easy and efficient. In addition, it is discovered that the detent force of PMTLG decreases dramatically after an adoption of the detent force minimization technique. The analysis results will provide useful reference for PMTLG design and optimization. Finally, after optimization of air-gap leakage flux coefficient and detent force, a PMTLG is built and experimented.

Received 12 April 2014, Accepted 5 June 2014, Scheduled 16 June 2014
* Corresponding author: Haitao Yu (htyu@seu.edu.cn).
The authors are with the School of Electrical Engineering, Southeast University, Jiangsu, China.

2. ANALYTICAL MODEL

In order to get a desirable analytical expression of air-gap leakage flux coefficient and make a detailed analysis of longitudinal end flux's influence on the detent force of PMTLG, an unsaturated reluctance model considering longitudinal end flux's influence is adopted. Figure 1(a) shows the basic structure of PMTLG, and Figure 1(b) shows the reluctance model of PMTLG.

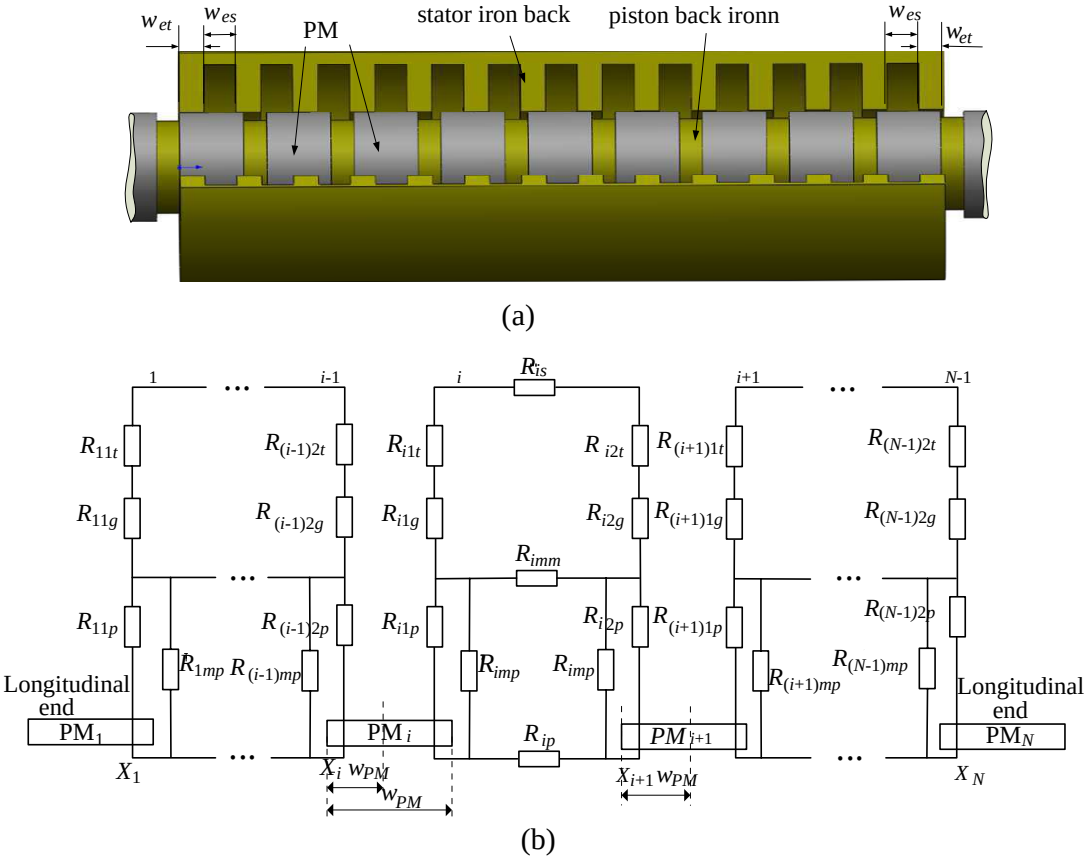

Figure 1. (a) Basic structure of PMTLG. (b) Reluctance model of PMTLG.

2.1. Air-Gap Leakage Flux Coefficient

Figure 2 shows part of flux distribution of PMTLG model. From Figure 2, it can be concluded that there are two parts of air-gap leakage flux; magnet-air-piston flux Φ_{MP} and magnet-air-magnet flux Φ_{MM}.

Figure 3 shows the electrical analogue of equivalent magnetic circuit in Figure 2, and the variables are listed as follows:

R_s reluctance of stator back iron;

R_g reluctance of air-gap;

R_{mm} reluctance of magnet-air-magnet;

R_{mp} reluctance of magnet-air-piston;

R_p reluctance of piston back iron;

Φ_g air-gap flux of one permanent magnet pole;

Φ_M flux source of one permanent magnet pole.

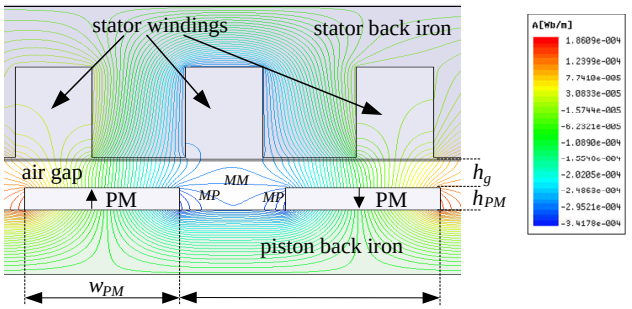

Figure 2. Part of flux distribution of PMTLG model.

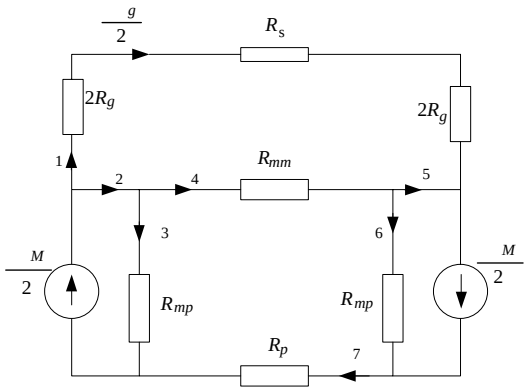

Figure 3. Electrical analogue of equivalent magnetic circuit in Figure 2.

For the back irons of PMTLG are unsaturated, the reluctances R_s and R_p can be ignored with respect to R_g. According to Kirchhoff's law, the matrix equation of Figure 3 can be written as

$$\begin{bmatrix} 4R_g & 0 & 0 & -R_{mm} & 0 & 0 & 0 \\ 0 & 0 & R_{mp} & -R_{mm} & 0 & -R_{mp} & 0 \\ 1 & 1 & 0 & 0 & 0 & 0 & 0 \\ 0 & -1 & 1 & 1 & 0 & 0 & 0 \\ 0 & 0 & 0 & -1 & 1 & 1 & 0 \\ 1 & 0 & 0 & 0 & 1 & 0 & 0 \\ 0 & 0 & 0 & 0 & 0 & 1 & -1 \\ 0 & 0 & 1 & 0 & 0 & 0 & 1 \end{bmatrix} \begin{bmatrix} \frac{\Phi_g}{2} \\ \Phi_2 \\ \Phi_3 \\ \Phi_4 \\ \Phi_5 \\ \Phi_6 \\ \Phi_7 \end{bmatrix} = \begin{bmatrix} 0 \\ 0 \\ \frac{\Phi_M}{2} \\ 0 \\ 0 \\ \frac{\Phi_M}{2} \\ -\frac{\Phi_M}{2} \\ \frac{\Phi_M}{2} \end{bmatrix} \tag{1}$$

Solving Equation (1), the air-gap flux Φ_g and flux source Φ_M can be obtained, and the air-gap leakage flux coefficient $k = \Phi_M/\Phi_g$ can be described as

$$k = \frac{\Phi_M}{\Phi_g} = 1 + 2\frac{R_g}{R_{mp}} + 4\frac{R_g}{R_{mm}} \tag{2}$$

The expression of reluctance in an air-gap magnetic circuit can be expressed as

$$R_g = \frac{LH}{AB} = \frac{L}{A\mu_0} \tag{3}$$

L length of air-gap magnetic circuit;
H field intensity of air-gap magnetic circuit;
A cross section of air-gap magnetic circuit;
B flux density of air-gap magnetic circuit;
μ_0 air-gap permeability.

For the above PMTLG model, R_g can be described as

$$R_g = \frac{h_g}{\mu_0 w_{PM} \pi r_{PM}} \tag{4}$$

R_{mm} and R_{mp} are calculated from the circular-arc straight-line permeance model [6], and depicted as follows:

$$R_{mp} = \frac{h_{PM} + \pi h_g}{\mu_0 h_g \pi r_{PM}} \tag{5}$$

$$R_{mm} = \frac{(\tau - w_{PM}) + \pi h_g}{\mu_0 h_g \pi r_{PM}} \tag{6}$$

where r_{PM} is equal to the outside diameter of PM, w_{PM}, τ, h_g and h_{PM} are shown in Figure 2.

2.2. Longitudinal End Flux's Influence on the Detent Force of PMTLG

Figure 1(b) consists of N PMs and $N-1$ flux paths, and every PM's flux is divided into two flux paths to connect with the left and right PM. Flux distribution parameter X_i indicates the portion of PM's flux connected with left or right flux path. Thus, the flux distribution parameters can be written as $X_{i+1} = 1 - X_i$. Every flux path consists of reluctance R and magnetomotive force F_{PM}, and the amplitude of flux Φ_i can be described as

$$\Phi_i = \frac{2F_{PM}}{R} = \frac{2H_c h_{PM}}{(R_{i1p} + R_{i1g} + R_{i1t} + R_{i2p} + R_{i2g} + R_{i2t} + R_{ip} + R_{is})} \tag{7}$$

where H_c is the coercivity of permanent magnet.

The reluctance model is unsaturated, thus the stator reluctance and piston reluctance can be neglected, and Equation (7) may be rewritten as

$$\Phi_i = \frac{2F_{PM}}{R} = \frac{2H_c h_{PM}}{(R_{i1p} + R_{i1g} + R_{i2p} + R_{i2g})} \tag{8}$$

where

$$R_{i1p} = \frac{h_{PM}}{\mu_0 \mu_{PM} \pi 2 r_{PM} (1 - X_i) w_{PM}} \tag{9}$$

$$R_{i1g} = \frac{h_g}{\mu_0 \pi 2 r_{PM} (1 - X_i) a_i w_{PM}} \tag{10}$$

$$R_{i2p} = \frac{h_{PM}}{\mu_0 \mu_{PM} \pi 2 r_{PM} X_{i+1} w_{PM}} \tag{11}$$

$$R_{i2g} = \frac{h_g}{\mu_0 \pi 2 r_{PM} X_{i+1} a_i w_{PM}} \tag{12}$$

where μ_{PM} is the PM's relative magnetic permeability and a_i the polar arc factor.

According to $\rho = B^2/(2\mu) = (\Phi/S)^2/(2\mu)$, where ρ is the magnetic energy density and S is the cross section of magnetic circuit, the magnetic energy of every flux path can be expressed as

$$U_i = \rho_i V_i = \frac{1}{2\mu} \left(\frac{\Phi_i^2}{(1 - X_i)(w_{PM} \pi 2 r_{PM})^2} + \frac{\Phi_i^2}{X_{i+1}(w_{PM} \pi 2 r_{PM})^2} \right) (w_{PM} \pi 2 r_{PM} h_{PM}) \tag{13}$$

Substitute Equation (8) into Equation (13), the total magnetic energy of PMTLG can be described as

$$U_{total} = \sum_{i=1}^{N-1} \frac{1}{2\mu} \frac{h_{PM}}{w_{PM} \pi 2 r_{PM}} \frac{4 (H_c h_{PM})^2}{(R_{i1p} + R_{i1g} + R_{i2p} + R_{i2g})^2} \left(\frac{1 - X_i + X_{i+1}}{(1 - X_i) X_{i+1}} \right) \tag{14}$$

Generally, when PMTLG's polar arc factor $a_i = 0.6 \sim 0.8$, the flux variation in stator is similar to sinusoidal. Thus the detent force of PMTLG can be obtained by the derivative of magnetic energy U_{total} with respect to position x

$$F = \frac{\partial U_{total}}{\partial x} = \sum_{i=1}^{N-1} \frac{1}{2\mu} \frac{h_{PM}}{w_{PM} \pi 2 r_{PM}} \frac{4 (H_c h_{PM})^2}{(R_{i1p} + R_{i1g} + R_{i2p} + R_{i2g})^2} \left(\frac{1 - X_i + X_{i+1}}{(1 - X_i) X_{i+1}} \right) \frac{\partial (\sin(x))^2}{\partial x} \tag{15}$$

Equation (15) indicates that the detent force w_{es} can be decreased by modifying the flux distribution parameter X_1 and X_N, which will be further discussed in Section 3.

3. FEA VERIFICATION

3.1. FEA Verification of Air-Gap Leakage Flux Coefficient

FEA is adopted to verify the validity of analytical expression (Equation (2)). Figure 4(a) shows the minimum air-gap leakage flux coefficientk_1, where slot's center line aligns with interpolar space. Figure 4(b) shows the maximum air-gap leakage flux coefficient X_1, where tooth's center line aligns

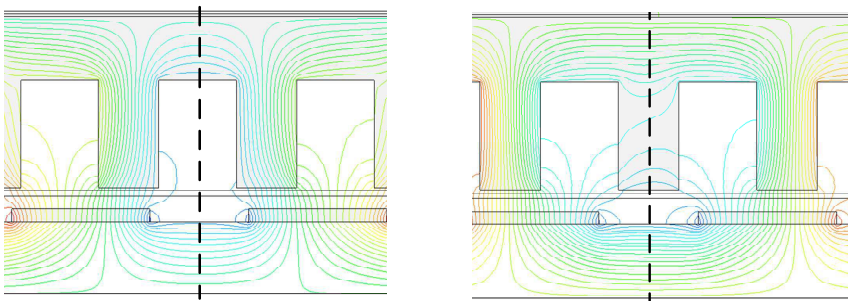

(a) (b)

Figure 4. (a) Minimum leakage flux k_1. (b) Maximum leakage flux k_2.

Table 1. Calculation results for w_{PM} (w_{es} = 1 mm, h_{PM} = 2 mm, τ = 49 mm).

w_{PM}	k_3 (FEA)	k (Analytical)	Error (%)
19.6 mm	1.100123	1.026118	6.7
24.4 mm	1.096621	1.021851	6.8
29.4 mm	1.090630	1.019213	6.5
34.3 mm	1.075121	1.017877	5.3
39.2 mm	1.050557	1.017808	3.1
44.1 mm	1.032275	1.020100	1.2

Table 2. Calculation results for h_{PM} (h_g = 2 mm, w_{PM} = 34.3 mm, τ = 49 mm).

h_{PM}	k_3 (FEA)	k (Analytical)	Error (%)
2 mm	1.077982	1.050389	2.6
3 mm	1.063940	1.047355	1.6
4 mm	1.053007	1.044912	0.8
5 mm	1.044883	1.042902	0.2
6 mm	1.038939	1.041219	0.2
7 mm	1.034527	1.039790	0.5

Table 3. Calculation results for h_g(h_{PM} = 2 *mm*, w_{PM} = 34.3 mm, τ = 49 mm).

h_g	k_3 (FEA)	k (Analytical)	Error (%)
1 mm	1.075121	1.017877	5.3
1.5 mm	1.100092	1.033062	6.1
2 mm	1.126176	1.050389	6.7
2.5 mm	1.143684	1.069300	6.5
3 mm	1.164234	1.089439	6.4
3.5 mm	1.190026	1.110560	6.7
4 mm	1.211762	1.132480	6.5

with interpolar space. Obviously, air-gap leakage flux coefficient $k_3 = (k_1 + k_2)/2$ is more accurate, closer to actual value. Table 1, Table 2 and Table 3 give the calculation results. From these Tables, it can be concluded that the maximum error (error=|FEA-Analytical|/FEA $*$ 100%) between FEA and analytical expression Equation (2) is about 6.8%.

3.2. FEA Verification of Amplitude of Detent Force

FEA is also adopted to verify the amplitude of detent force (Equation (15)). Table 4 shows the specifications of PMTLG, and Figure 5 shows the detent force results.

From Figure 5 it can be concluded that the amplitude of analytical results is in agreement with the FEA ones. However, Figure 5 also shows other discrepancies between the analytical and FEA results, which are mainly due to three mechanisms:

1) The leakage flux, such as magnet-air-piston flux and magnet-air-magnet flux, is not taken into account in Equation (15).

Table 4. Specifications of PMTLG.

	Item	Symbol	Value(Unit)
Stator	Pole pitch	τ	49 (mm)
	Slot pitch	τ_s	32 (mm)
	Slot width	w_s	18 (mm)
	No. of winding/phase		260
	Iron material		D23
	Winding material		Copper
Permanent magnets	Height	h_{PM}	4 (mm)
	Width	w_{PM}	36 (mm)
	Material		NdFe35
Air gap	Air gap width	h_g	2 (mm)

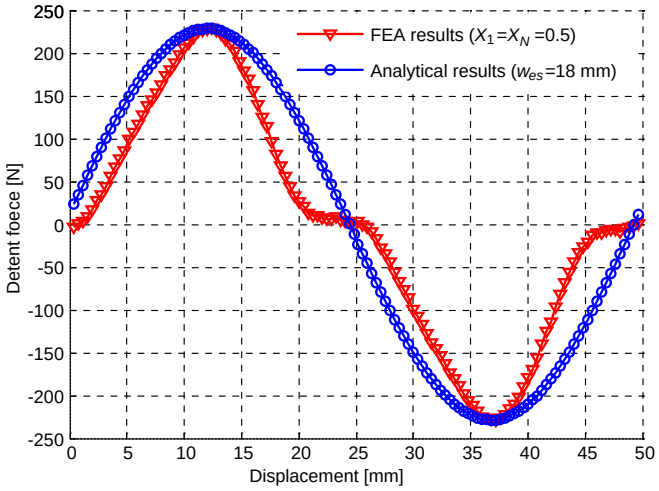

Figure 5. Amplitude verification of detent force (w_{es} is end slot width).

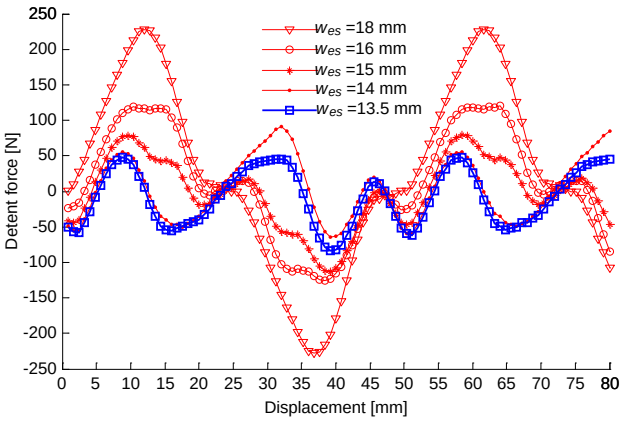

Figure 6. Detent force reduction according to the end slot width w_{es}.

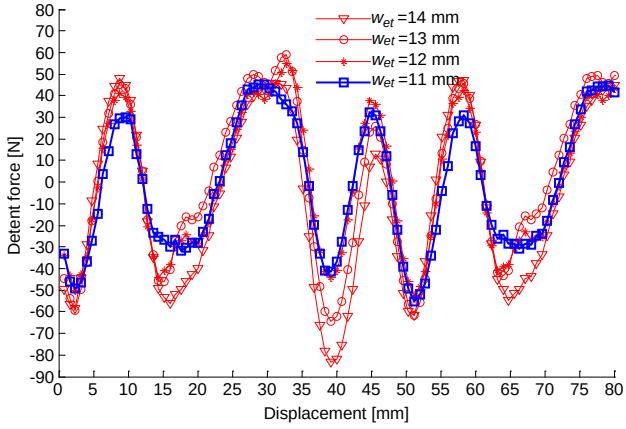

Figure 7. Detent force further reduction by modifying the end tooth width w_{et}.

2) In FEA, flux variation in stator back iron is not absolutely sinusoidal due to the structure of PMLTG.
3) In FEA, some of teeth fringes are saturate periodically when piston moves along the stator.

3.3. The Deduced Detent Force Minimization Technique

Equation (15) indicates that detent force of PMTLG can be reduced by modifying the distribution parameters X_1 and X_N through changing the end slot width w_{es}, and the FEA verification results are illustrated in Figure 6. For the specifications in Table 4 (the end slot width $w_{es} = 18\,\text{mm}$), the peak-to-peak detent force is 457.2 N. When it is with $w_{es} = 13.5\,\text{mm}$, the peak-to-peak detent force is 123.6 N. This indicates 73% detent force has been removed.

In addition, the detent force of PMTLG can be reduced even further by changing the end tooth width w_{et}. After the detent force reduction by end slot width w_{es}, Figure 7 shows the detent force further reduction by end tooth width w_{et} When it is with $w_{et} = 11\,\text{mm}$, the peak-to-peak detent force is 94.4N, which indicates 79.4% detent force has been removed.

4. THE LONGITUDINAL END EFFECT ON THE BACK-EMF OF PMTLG

Actually, after changing the end tooth width w_{et} and end slot width w_{es}, the harmonic components of back-EMF will be increased. Therefore, some methods should be adopted to reduce the harmonic components of back-EMF, such as changing the number of windings distribution, reducing the pole pitch and so on Figure 8 shows the windings distribution of PMTLG, where there are two phase windings in each slot. According to Table 4 (the end slot width $w_{es} = 13.5\,\text{mm}$ and end tooth width $w_{et} = 11\,\text{mm}$), the three phase back-EMF waveforms are high harmonic components and asymmetrical, as shown in Figure 9(a). However, when the pole pitch is reduced to $\tau = 25\,\text{mm}$ and the number of windings of phase B increases to 268, the phase back-EMF waveforms are nearly symmetrical and the harmonic components are decreased, as shown in Figure 9(b).

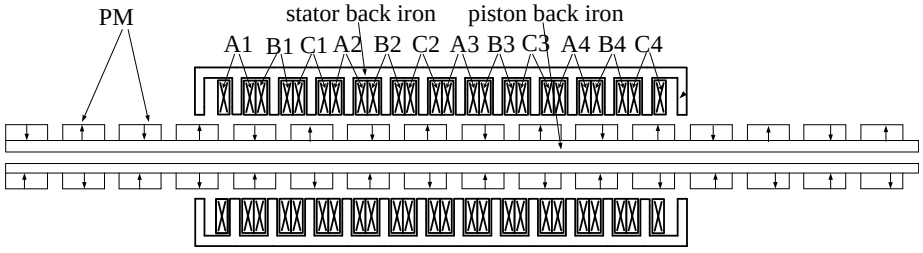

Figure 8. The windings distribution of PMTLG.

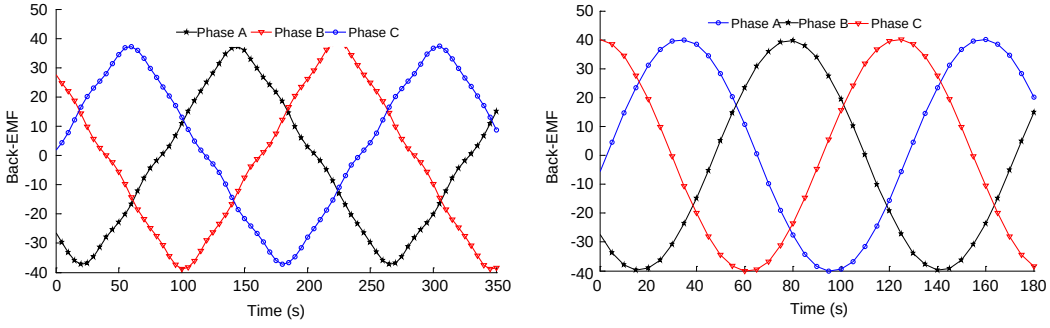

Figure 9. (a) Back-EMF of PMTLG for the specifications in Table 4. (b) Back-EMF of PMTLG for the pole pitch reduced to $\tau = 25\,\text{mm}$ and the number of windings of phase B increase to 268.

5. RESULTS

After air-gap leakage flux coefficient and detent force optimization, a prototype of PMTLG is built, as shown in Figure 10. The air-gap leakage flux coefficient is 1.016963 by Equation (2), and the detent force result is shown in Figure 11.

Figure 10. (a) Prototype of PMTLG. (b) Piston of PMTLG.

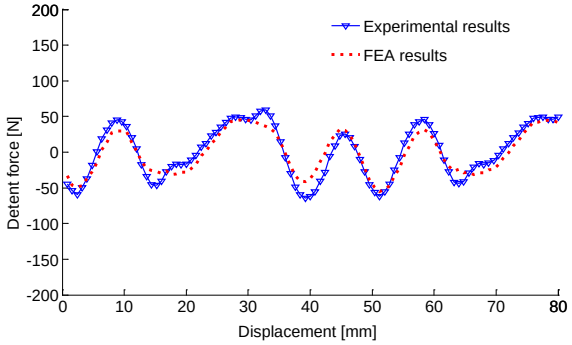

Figure 11. Detent force results.

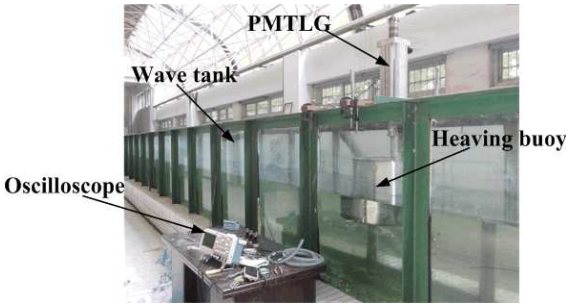

Figure 12. The wave energy conversion system.

Further, the prototype of PMTLG is installed in a wave tank, as shown in Figure 12. In the experiment, the PMTLG's piston can be driven by wave force through the vertical motion of heaving buoy. Therefore, the permanent magnets of piston produce a varying flux, which induces voltages in the stator windings. In such a case that the PMTLG's piston is directly coupled to wave force instead of hydraulic or pneumatic system, the wave energy conversion system cost and complexity are reduced.

According to the wave propagating in sinusoidal trace (wave height is 0.3 m and wave period is 2 s), Figure 13(a) shows the measured no-load three-phase voltages. Because of the inconstant vertical speed of wave, the measured no-load three-phase voltages are non-sinusoidal. Figure 13(b) shows the measured load three-phase voltages (the resistance is 12 Ω). From Figure 13, it can be seen that the voltage converters (rectifiers and inverters) are required before the wave energy ultimately used.

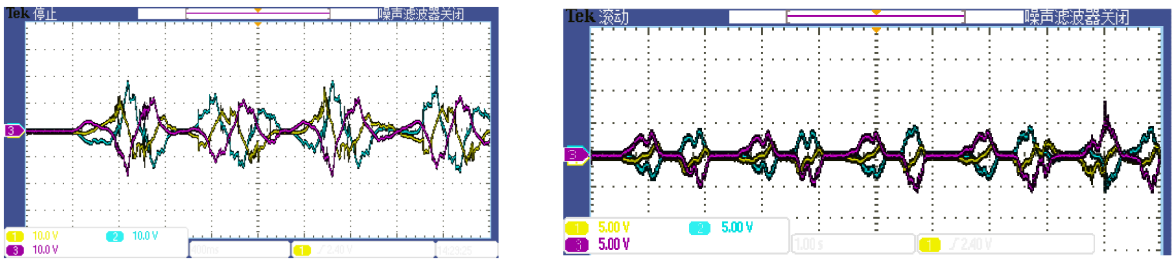

Figure 13. (a) The no-load voltages (each unit of the horizontal-axis and vertical-axis are 100 ms and 10 V respectively). (b) The load voltages (each unit of the horizontal-axis and vertical-axis are 1 s and 5 V respectively).

6. CONCLUSIONS

The analysis results show that the analytical expression of air-gap leakage flux coefficient should benefit the optimization of PMTLG. Moreover, longitudinal end flux's influence on the detent force of PMTLG is analyzed, and a detent force minimization technique is deduced from the analysis results. The analysis and experimental results will bring benefits to PMTLG design and future works concerning conversion of ocean wave energy into electrical energy.

ACKNOWLEDGMENT

This work is financially supported by the Scientific Research Foundation of Graduate School of Southeast University (YBJJ1416).

REFERENCES

1. Prudell, J., M. Stoddard, E. Amon, T. K. A. Brekken, and A. V. Jouanne, "A permanent-magnet tubular linear generator for ocean wave energy conversion," *IEEE Trans. Ind. Applicant*, Vol. 46, No. 6, 2392–2400, 2010.
2. Leijon, M., H. Bernhoff, O. Ågren, J. Isberg, J.,Sundberg, M. Berg, K. E. Karlsson, and A. Wolfbrandt, "Multiphysics simulation of wave energy to electric energy conversion by permanent magnet linear generator," *IEEE Trans. Energy Conversion*, Vol. 20, No. 1, 219–224, 2005.
3. Danielsson, O. and M. Leijon, "Flux distribution in linear permanent-magnet synchronous machines including longitudinal end effects," *IEEE Trans. Magn.*, Vol. 43, No. 7, 3197–3201, 2007.
4. Wang, J., D. Howe, and G. W. Jewell, "Fringing in tubular permanent magnet machines: Part I. Magnetic field distribution, flux linkage, and thrust force," *IEEE Trans. Magn.*, Vol. 39, No. 6, 3507–3516, 2003.
5. Tsai, W. and T. Chang, "Analysis of flux leakage in a brushless permanent-magnet motor with embedded magnets," *IEEE Trans. Magn.*, Vol. 35, No. 1, 543–547, 1999.
6. Hanselman, D. C., *Brushless Permanent-magnet Motor Design*, McGraw-Hill, New York, 1994.
7. Qu, R. and T. A. Lipo, "Dual-rotor, radial-flux, toroidally-wound, permanent-magnet machines," *Conf. Rec., IEEE-IAS Annul. Meeting*, Vol. 2, 1281–1288, 2002.
8. Faiz, J. and M. E. Salari, "Comparison of the performance of two direct wave energy conversion systems: Archimedes wave swing and power buoy," *J. Marine. Sci. Appl.*, Vol. 10, 421–428, 2011.
9. Wang, J., M. Inoue, Y. Amara, and D. Howe, "Cogging-force-reduction techniques for linear permanent-magnet machines," *IEE Proc. — Electr. Power Appl.*, Vol. 152, No. 3, 731–738, 2005.
10. Lee, J., H. W. Lee, Y. D.,Chun, M. Sunwoo, and J. P. Hong, "The performance prediction of controlled-PMLSM in various design schemes by FEM," *IEEE Trans. Magn.*, Vol. 36, No. 4, 1902–1905, 2000.
11. Ahmad, M. E., H. W. Lee, and M. Nakaoka, "Detent force reduction of a tubular linear generator using an axial stepped permanent magnet structure," *Journal of Power Electronics*, Vol. 6, No. 4, 290–296, 2006.
12. Bianchi, N., S. Bolognani, and A. D. F. Cappello, "Reduction of cogging force in PM linear motors by pole-shifting," *IEE Proc. — Electr. Power Appl.*, Vol. 152, No. 3, 703–709, 2005.
13. Ji, J., J. Zhao, W. Zhao, Z. Fang, G. Liu, and Y. Du, "New high force density tubular permanent-magnet motor," *IEEE Trans. Appl. Supercon.*, Vol. 24, No. 3, 5200705, 2014.
14. Ji, J., S. Yan, W. Zhao, G. Liu, and X. Zhu, "Minimization of cogging force in a novel linear permanent-magnet motor for artificial hearts," *IEEE Trans. Magn.*, Vol. 49, No. 7, 3901–3904, 2013.